An energy tunable continuous 2³S₁ positronium beam

D. M. Newson ⓘ ; T. J. Babij; D. B. Cassidy ✉ ⓘ

Check for updates

CrossMark

View Online

Export Citation

Articles You May Be Interested In

A pulsed positronium beam using a positron buffer gas trap

Rev Sci Instrum (March 2020)

Positronium Formation in Gases

Journal of Applied Physics (May 2004)

Fundamental Physics with Cold Positronium

AIP Conference Proceedings (August 2008)

Review of Scientific Instruments

AIP Publishing

An energy tunable continuous 2³S₁ positronium beam

View Online   Export Citation   CrossMark

D. M. Newson, [ID] T. J. Babij, and D. B. Cassidy[a) [ID]

AFFILIATIONS

Department of Physics and Astronomy, University College London, Gower Street, London WC1E 6BT, United Kingdom

[a)]Author to whom correspondence should be addressed: d.cassidy@ucl.ac.uk

ABSTRACT

We describe the experimental production of a beam of 2^3S_1 positronium (Ps) atoms obtained from charge-exchange collisions between a positron beam and Xe held in a gas cell. The angular divergence of the emitted Ps beam was recorded using two position sensitive detectors located at different distances from the gas cell. The fraction of the Ps beam produced in the 2^3S_1 level was measured via the change in the Ps count rate after driving the $2^3S_1 \rightarrow 2^3P_2$ transition with microwave radiation; with optimal experimental parameters, we estimate that up to 10% of the Ps beam is formed in the 2^3S_1 state. The measured properties of the beam were used to evaluate the feasibility of using the system for precision spectroscopy of the $n = 2$ Ps fine structure using Ramsey interferometry.

I. INTRODUCTION

Positronium (Ps), the electron-positron bound-state,[1] is of fundamental interest as a testing ground for QED theory,[2] a probe of solid state materials,[3] and a projectile for scattering measurements.[4] The simplicity of Ps also allows for its use as a possible probe of physics beyond the Standard Model.[5] For many measurements involving Ps, for example laser spectroscopy,[6] low-energy Ps atoms are required. These may be obtained by implanting positrons into various solid-state targets[7] that generate Ps at either near thermal ($\approx$50 meV)[8] or few eV[9] energies, depending on the exact formation mechanism. However, these methods offer no practical way to tune the Ps energy over a wide range; limited energy tuning can be obtained using some meso-porous silica films[10] in which Ps thermalization depends on the positron implantation energy,[11] but the Ps energy spread is generally broad with respect to the mean Ps energy, and the tuning range is restricted to $\approx$0.05–1 eV. The emission of Ps with a narrower energy spread has been observed using Metal Organic Framework materials,[12] but this mechanism does not allow for energy tuning. Guided beams of highly excited (Rydberg) Ps atoms[13] can be produced using electrostatic field gradients.[14] In principle, time-varying electric fields can be used to directly control Rydberg Ps velocities,[15] but this has not yet been experimentally demonstrated.

For scattering measurements, an energy tunable beam is required; these may be generated in various ways, such as glancing angle positron scattering from surfaces,[16] charge-exchange of a continuous[17] or pulsed[18] positron beam with low-density gases, or pulsed photo-detachment of negative Ps⁻ ions.[19] The glancing angle method works in an energy range of up to $\approx$100 eV and, in principle, can be continuous or pulsed, although only the former has been experimentally demonstrated.[16] The photo-detachment method can produce energetic beams in the range of 0.2–3.3 keV by accelerating ions in a strong electric field prior to the photo-detachment. This method employs an alkali-metal covered surface for ion production with ~1% efficiency, and since a pulsed laser is required, it can only be used with a pulsed beam.[20] Ps formed by the charge-exchange of a positron beam with low-density gases has been used to investigate the scattering of Ps from atoms and molecules at University College London (UCL) for many years,[21–23] taking advantage of the natural propensity for Ps production in the forward direction at intermediate energies (1–250 eV). In this method, Ps is produced in a gas cell with an energy distribution set by that of the incident positron beam. Different gases and pressures can be used to optimize Ps production over a particular energy range.[24] In general, Ps produced in this way is predominantly formed in the ground state ($n = 1$, where n is the principle quantum number) and distributed according to the available spin (S) multiplicities ($2S + 1$); i.e., 75% of atoms are

produced in the $S = 1$ triplet states (1^3S_1) and 25% are produced in the $S = 0$ singlet states (1^1S_0). The triplet and singlet states have lifetimes against annihilation of 142 ns and 125 ps, respectively.[5] As a result, the singlet states do not live long enough to travel out of the gas cell, and the resulting Ps beam is composed exclusively of triplet state atoms, primarily in the ground-state.

The production of excited-state Ps atoms, specifically $n = 2$ states, has been identified in low-density Ne, Ar, Xe, and H_2 gases.[25,26] In the case of Xe, Murtagh *et al.*[26] reported that up to (26 ± 9)% of all Ps atoms formed were in the 2P levels. In that work, the formation of excited state Ps atoms was detected via the emission of Lyman alpha photons ($\lambda = 243$ nm) following radiative decay to the ground state: $2^3P_J \rightarrow 1^3S_1$. Because 2P states decay quickly, with a mean radiative lifetime of 3.2 ns,[27] they do not exit the gas cell in the excited-state. Owing to its stochastic nature, excited-state production can be expected to occur across the entire $n = 2$ manifold, and the production of 2P atoms implies that 2S states will also be produced. Self-annihilation is highly suppressed for the 2P states,[28,29] which decay exclusively via fluorescence. Conversely, S states are radiatively metastable, according to electric dipole selection rules,[30] but can decay via self-annihilation with a lifetime that scales[27] with n^3. Therefore, the mean lifetime of 2^1S_0 atoms is eight times longer than that of 1^1S_0 atoms (i.e., 1 ns), whereas the mean annihilation lifetime of 2^3S_1 atoms is 1136 ns, although this may be different if external electric or magnetic fields are present.[31] Therefore, one can expect a beam of long-lived 2^3S_1 atoms to be emitted from a Xe filled gas cell irradiated with a positron beam under certain experimental conditions, namely with the appropriate incident positron beam energy and Xe gas pressure.

Here we show that this is indeed the case: we describe the production of a 2^3S_1 Ps beam using a modified version of the UCL Ps beam apparatus.[17] A Ps beam generated in a Xe gas cell was observed using microchannel plate (MCP) and delay line anode position sensitive detectors located at different positions, as described below. These detectors provided direct measurements of the Ps beam

intensity and also spatial information, allowing the transverse velocity distributions to be determined. The 2^3S_1 component of the Ps beam was measured via beam loss following microwave radiation induced transitions $2^3S_1 \rightarrow 2^3P_J \rightarrow 1^3S_1$ that transfer the long-lived 2^3S_1 population to the ground state and, therefore, reduce the fraction of atoms that reach the detector.

The motivation for this work is the implementation of a measurement scheme designed to perform spectroscopy of the Ps $n = 2$ fine structure using techniques based on the Ramsey method of separated oscillatory fields (SOF).[32] This methodology offers several advantages over previously used techniques[33,34] but cannot be used with low-energy Ps sources. In the planned experiments, a short-lived superposition-state comprising both 2S and 2P components will travel between two waveguides separated by a distance such that the flight time for near-thermal Ps atoms would be much longer than the lifetime against annihilation. A source of faster 2^3S_1 Ps atoms is therefore required to produce a useful signal using this technique.[35]

II. POSITRONIUM BEAM APPARATUS

A. Positronium beam production

The UCL Ps beam has been described in detail elsewhere.[36] Here we give a brief overview along with a description of various modifications to the system. A schematic representation of the present beamline is shown in Fig. 1. Fast β^+ particles produced through the decay of ^{22}Na were moderated by a thin film of Ne frozen directly onto the cooled ($\simeq 4$ K) source capsule.[37] In the moderation process, positrons rapidly lose energy via electron–hole production in the frozen Ne matrix until they reach the bandgap energy (≈ 20 eV), whereupon energy loss proceeds more slowly via phonon scattering, and un-thermalized (epithermal) positrons are emitted into the vacuum, typically with an energy spread on the order of 1 eV. Moderated positrons were accelerated by an electric
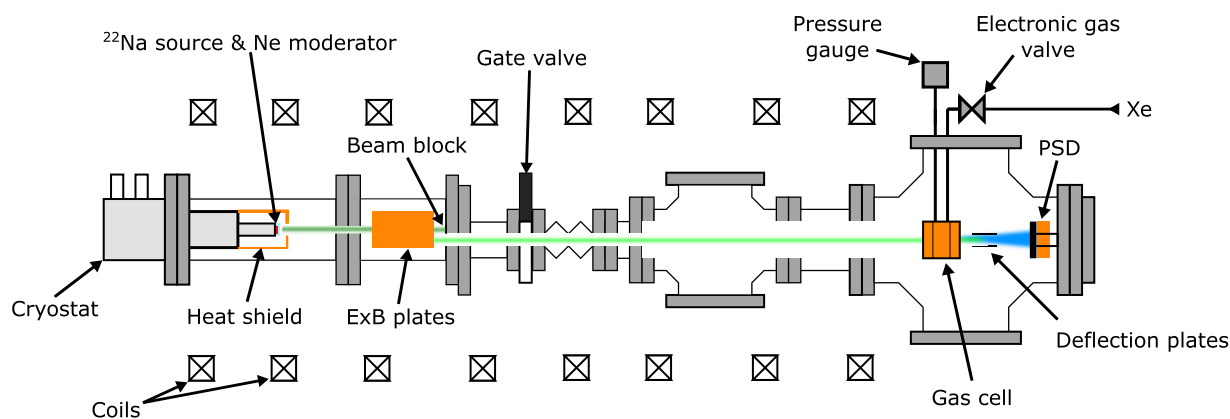

FIG. 1. Schematic representation of the apparatus. A slow mono-energetic positron beam is produced from a sodium-22 source using a biased Ne moderator, confined radially by a $\approx$100 G axial magnetic field. The positron beam is deflected off axis by a set of $E \times B$ plates, collimated to a diameter of 4 mm, and transported to the Ps production gas cell. Both ground and excited state Ps may be produced in the cell, depending on the beam energy and gas pressure. The positron and positronium beams are observed directly using a delay line anode position sensitive detector (PSD). For Ps measurements, the residual positron beam is deflected using a set of biased parallel plates. The green line represents the positron beam, and the blue shaded region represents the diverging positronium beam.

field created by a positive voltage applied to the source capsule, and were confined radially by an axial magnetic field of strength 2–5 mT. The positron beam was then deflected off-axis by an E ×B filter[38] to remove the line-of-sight between the source region and detector. The deflected beam was collimated by apertures to a diameter of ≈4 mm.

Ps production occurred in a gas cell, as indicated in Fig. 2. The gas cell consists of an interior region 20 mm in length, bounded by two cylindrical apertures of length 17 mm and diameter 4 mm. Gas flow into the cell was controlled by an electronic valve (Pfeiffer EVR-116), and the pressure was measured using a capacitance manometer (MKS 127A). A software-based proportional-integral-derivative (PID) loop was used to stabilize the gas pressure against temperature variations in the laboratory. For measurement of the Ps beam, the positron beam was deflected away from the detector by a set of parallel plates placed close to the exit aperture of the gas cell. The electrodes were 8×5 cm^2 in size and separated by 2 cm. The lower plate was grounded, and the bias on the upper plate was adjusted according to the positron beam energy in order to stop the beam using the minimum electric field. Therefore, the upper plate bias varied from +125 to +300 V, generating a static electric field ranging from 0.06 to 0.15 kV/cm. These fields were minimized to reduce 2^3S_1 beam loss via Stark mixing.[39]

Two different types of position sensitive detectors (PSDs) were used to characterize and cross check the Ps beam, namely Roent-Dek DLD40 and DLD80, which contain delay line anodes and 40 or 80 mm diameter MCPs, respectively. Measurements were made with the detectors placed at different distances of $z_{\mathrm{det}}^{40} = 219$ mm (DLD40) and $z_{\mathrm{det}}^{80} = 475$ mm (DLD80) from the center of the gas cell (see Fig. 2). Particle hits on the detectors were only registered as events if the MCP front and both delay lines (x and y) were all triggered. The front MCP plate was biased negative to repel stray electrons. Constant fraction discriminators were used to exclude electronic noise on all channels.
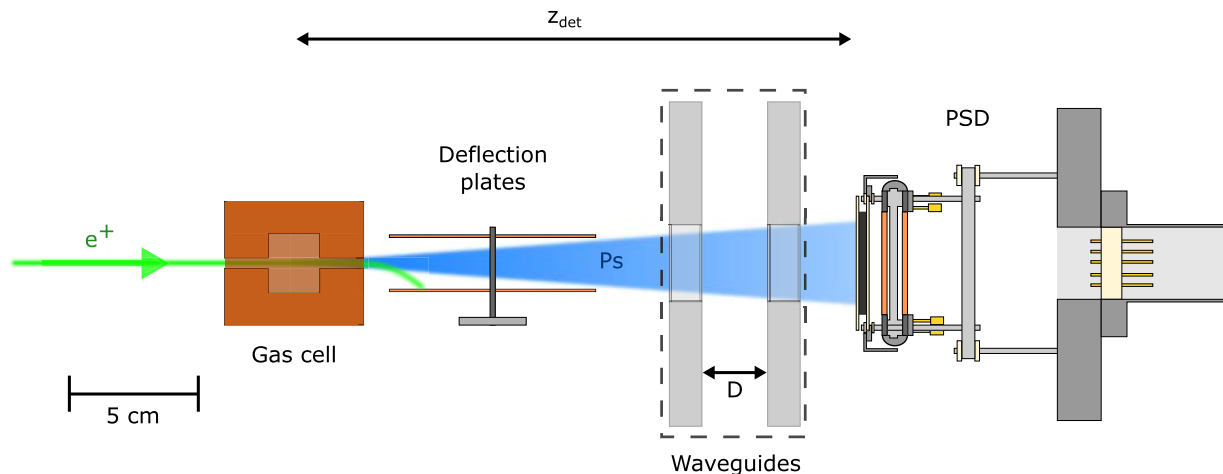

FIG. 3. Energy distribution of the positron beam measured using a retarding field analyzer. The dashed line is a Gaussian fit to the data with a FWHM of 1.3 eV.

Ps and Ps* were formed in the gas cell via the charge-exchange reaction

$$e^+ + \mathrm{Xe} \rightarrow \mathrm{Ps}^{(*)} + \mathrm{Xe}^+, \tag{1}$$
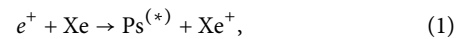
where Ps* represents Ps in the $n = 2$ excited state. The energy of the resulting Ps beam is given by

$$E_{\mathrm{Ps}} = E_+ - E_i + \left(\frac{E_B}{n^2}\right), \tag{2}$$

where E_+ is the energy of the incident positron beam, E_i is the ionization threshold of the production gas (12.13 eV for Xe), E_B is the ground state positronium binding energy (6.8 eV), and n is the Ps principal quantum number. Unless otherwise stated, all data presented below were taken with the Xe gas cell pressure set to 0.6 Pa and a positron beam energy of 40 eV, which are close to the optimal parameters for Ps beam production, as explained below.

FIG. 2. Scale representation of the gas cell, deflection plates, and PSD. The positron and positronium beams traveling from left to right are highlighted in green and blue, respectively. Experiments were performed using two different position sensitive detectors, the DLD40 (diameter 40 mm) and DLD80 (diameter 80 mm), located at distances z_{det} (219 and 467 mm, respectively) from the center of the gas cell. The DLD40 arrangement is shown here. Also shown are two waveguides separated by a distance D that will be used in future Ramsey separated oscillatory field interferometry experiments, as discussed in Sec. V.
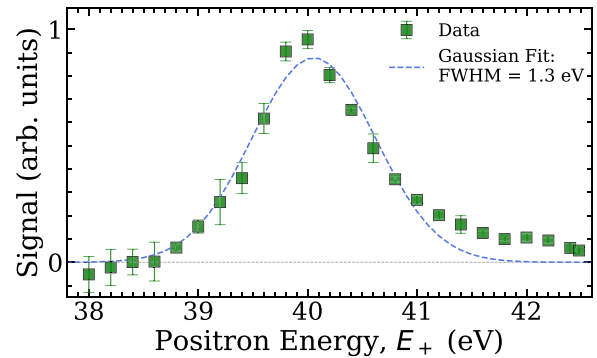
29 August 2023 19:17:37

The Ps and Ps* beams will differ in energy by ≈ 5.1 eV, meaning that they could be distinguished by their time-of-flight to the detector. However, this would require time-tagging the incident positron beam,[40] which would considerably reduce the count rate. The energy spread of the Ps beam is determined primarily by that of the incident positron beam, which is itself determined by the positron moderation process. The positron beam energy spread has been directly measured using a retarding field analyzer (i.e., a set of grids) and a channel electron multiplier placed after the gas cell. The results of this measurement are shown in Fig. 3. The positron beam energy distribution may be approximately represented by a Gaussian function, with a full width at half maximum (FWHM) of ≈ 1.3 eV and a peak energy ≈ 2 eV above that of the potential applied to the source and moderator, which in this case was 38 V.

B. Positronium beam properties

The positron and positronium beam profiles, as measured by the DLD40 detector, are shown in Figs. 4(a) and 4(b), respectively. The total background-subtracted positron and Ps beam
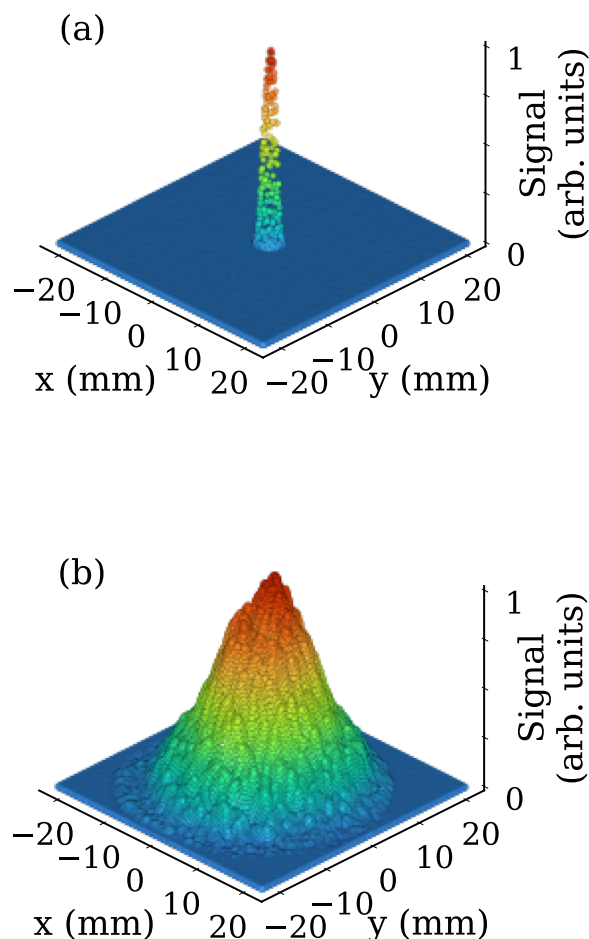
(a)

(b)

FIG. 4. Normalized positron (a) and Ps (b) beam profiles measured using the DLD40 detector as described in the text. The image shown in (a) was acquired in 186 s, and the image shown in (b) was acquired in 6.3 h.

count rates for these measurements were $C_{Ps} = 27.8 \pm 0.1$ s^{-1} and $C_{e^+} = 48\,823 \pm 16$ s^{-1}, respectively. Similar measurements were performed with the DLD80, yielding $C_{Ps} = 18.6 \pm 0.1$ s^{-1} and $C_{e^+} = 47\,537 \pm 69$ s^{-1}. The count rates measured on the two detectors are not directly comparable because (1) the detection efficiencies are not necessarily the same for both devices, and (2) the fraction of surviving atoms reaching the detectors will be different. The background, which mostly comprised dark counts in the detector and gamma-rays from surrounding annihilation events, was measured with no gas in the Xe cell. The background rates associated with the measurements described above were $C_{Bk} \approx 20$ s^{-1} for both the DLD40 and DLD80 detectors.

The distance that atoms must travel to reach the detectors will depend on exactly where the atoms are created in the gas cell; however, since this distance is much longer than the dimensions of the cell, we assume that all atoms are created in the center of the cell and that the longitudinal flight distance is always given by z_{det} (see Fig. 2). The fraction of Ps atoms that reach the detector before decaying from their initial states is $f_i = \exp(-t/\tau)$, where t is the flight time and τ is the limiting lifetime for a given Ps state (i.e., 142 ns and 1136 ns for the 1^3S_1 and 2^3S_1 levels, respectively).

The kinetic energies, and hence flight times, for ground and excited state Ps atoms will be different; for on-axis ground (excited) Ps atoms produced from a 40 eV positron beam, t is ~87 ns (96 ns), and f_i at the position of the DLD40 detector is 51% (92%). The corresponding numbers for the DLD80 are flight times of 205 ns (189 ns) and surviving fractions of 26% (83%). However, for the 2^3S_1 case, f_i is not measured directly by the PSD because excited Ps atoms that decay to the ground state may still be detected before they self-annihilate, meaning that, to properly interpret the corresponding 2^3S_1 signal, the count rate has to be adjusted to take this into account. In order to do so, it is necessary to know where the transitions take place; this is discussed in Sec. IV.

The detector positions were chosen such that the entirety of the divergent Ps beam was encompassed within the diameter of the PSD. The angular divergence of the Ps and Ps* beams was set by the relevant differential Ps formation cross-sections (which are not known for Xe) and the geometry of the exit aperture of the gas cell (pencil angle $\simeq 4.2°$ from the middle of the cell). The fraction of positrons entering the gas cell that undergo charge exchange reactions and form Ps depends on the experimental conditions, such as beam energy, gas species, or gas pressure. Based on the DLD40 and DLD80 data described earlier, the Ps formation fractions are both $\approx 0.2\%$ after accounting for in-flight annihilation. We note that this Ps formation fraction is broadly consistent with previous measurements.[24]

Imaging the Ps beam makes it possible to determine the transverse velocity components (v_x, v_y) if a few assumptions are made. Background measurements were performed with the positron beam deflection field on and no gas in the Ps production cell. The background obtained in this way was different from that obtained with the positron beam blocked because of a small but non-zero annihilation radiation signal emanating from the beam deflection plates. To extract the Ps velocity distributions from the background subtracted images, 2D Gaussian functions were fitted to the images from the PSD to determine the center of the Ps beam. The images were then shifted such that the center coincided with the (x, y) coordinates (0,0). This was required to correct the misalignment of the gas cell
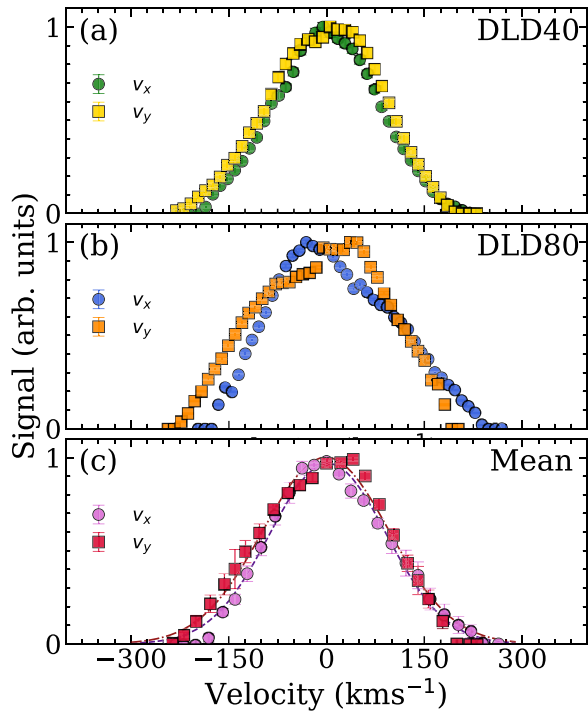
29 August 2023 19:17:37

FIG. 5. Transverse velocity distributions of the Ps beam as determined from the DLD40 (a) and DLD80 (b) detectors, as described in the text. Panel (c) shows the mean distributions along with Gaussian fits (lines) to each case.

and the detectors. This procedure assumes that the beam profiles are symmetric, which is not completely correct because of distortions in the incident positron beam. The transverse velocity components are given by

$$v_x = \frac{v_\parallel x}{z_{\text{det}}}, \qquad v_y = \frac{v_\parallel y}{z_{\text{det}}}, \qquad (3)$$

where (x, y) is a position on the PSD. We make the approximation $v_\parallel \approx \sqrt{E_{\text{Ps}}/m_e}$ since the longitudinal Ps velocity is much larger than the axial velocity components over the relevant energy range (10–120 eV). The velocity distributions obtained in this way for the DLD40 and DLD80 detectors are shown in Figs. 5(a) and 5(b), respectively. Asymmetries in the observed beam profiles are caused by asymmetries in the incident positron beam profile and spatial variations in the efficiency of the detectors, and so we take the mean of the two measurements to represent the Ps transverse velocity distributions, as shown in Fig. 5(c).

III. MICROWAVE SPECTROSCOPY

A. 2^3S_1 beam detection

The Ps beam, as measured on the DLD40 and DLD80 detectors, contains both 1^3S_1 and 2^3S_1 atoms. The excited state component of the Ps beam was identified by driving $2^3S_1 \rightarrow 2^3P_2$ transitions using microwave radiation. As discussed earlier, Ps atoms in 2^3P_J states decay radiatively to the ground state with a mean lifetime of 3.2 ns.

The presence of a magnetic field means that some atoms undergoing this process may decay to the short lived singlet ground state,[39] but the majority ($\geq 90\%$) will decay to the longer-lived triplet ground state, and some of these atoms may still travel to the detector and be counted. These atoms will be indistinguishable from atoms that remain in the 2^3S_1 level, and hence the apparent rate of microwave induced transitions will be lower than the actual rate. Nevertheless, this process will reduce the total count rate since the decay rates of the ground and excited states differ by a factor of 8.

Measurements were performed with and without microwave radiation present, and the corresponding background-subtracted count rates [S_{ON} and S_{OFF}] were used to generate the signal parameter S_B, given by

$$S_B = \frac{S_{\text{OFF}} - S_{\text{ON}}}{S_{\text{OFF}}}. \qquad (4)$$

This parameter represents the observed fractional change in the count rate caused by microwave radiation and is, therefore, a measure of the extent to which $2^3S_1 \rightarrow 2^3P_2$ transitions occur. Lineshapes were generated by measuring $S_B(\nu)$, where ν is the frequency of the microwave radiation.

Transitions were driven using free-space microwave radiation[42] in the frequency range 8.45–8.90 GHz, generated with a horn antenna (Pasternack PE9857/SF-15, WR-102, 15 dBi nominal gain). The radiation source was a signal generator (Keysight E8257D) connected to a low-noise amplifier (Microwave Amps AL7 LNA). The gain of the AL7 amplifier was 21 dB, and the maximum output power was $\simeq 1.4$ W. A Mini Circuits ZVE-3W-183+ amplifier was used to measure the saturation of the transition because it could provide up to 2.6 W. The AL7 was used for spectroscopic measurements because of its superior noise characteristics. The signal generator output power was varied over the measurement frequency range (including a small correction to account for variations in the gain of the horn antenna) so as to stabilize the horn output power. The frequency dependence of the horn gain was determined from a numerical calculation of the far-field distribution in free-space using the CST Studio software package.[43]

Measurements of S_B as a function of the microwave radiation frequency are shown in Fig. 6. For these measurements, the input power to the horn antenna was $P_{\text{input}} = 0.25$ or 1.20 W, as indicated. The resulting lineshapes were fitted to a Lorentzian function [$L(\nu)$] of the form

$$L(\nu) = C \frac{\frac{\Gamma}{2}}{(\nu - \nu_R)^2 + \left(\frac{\Gamma}{2}\right)^2}, \qquad (5)$$

where C is a constant related to the intensity of the transition, Γ is the full width at half maximum (FWHM), and ν_R is the resonance frequency of the transition. The natural width of the $2^3S_1 \rightarrow 2^3P_2$ transition is ≈ 50 MHz, predominantly determined by the 2^3P_2 radiative lifetime. The theoretical field-free transition frequency[41] is $\nu_2 = (8626.71 \pm 0.08)$ MHz; the parameter ν_R differs from ν_2 as it represents the resonance frequency of the transition in the presence of external electric or magnetic fields. Both of the measurements shown in Fig. 6 yield widths of ≈ 150 MHz and resonance frequencies ≈ 30 MHz above the theory value. As discussed below (see Sec. IV), we attribute these observations to the electric field caused by the positron beam deflector plates.
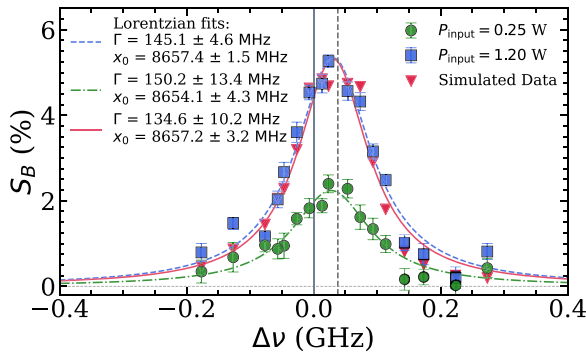
29 August 2023 19:17:37

FIG. 6. S_B for microwave frequencies in the range 8.45–8.90 GHz for P_{input} = 0.25 W (circles) and P_{input} = 1.20 W (squares). The dashed and dotted-dashed lines are Lorentzian fits with χ^2 of 1.97 and 0.79, respectively. The solid (red) line is the result of a simulation as described in Sec. III B. The solid vertical line at $\Delta\nu = 0$ corresponds to the theoretical field-free transition frequency (ν_2, see text).[41] The dashed vertical line at $\Delta\nu = +37$ MHz represents the Zeeman and Stark shifts expected from the experimental conditions, as explained in the text.

The observed lineshapes shown in Fig. 6 unequivocally demonstrate the presence of a 2^3S_1 beam. In order to estimate the excited state fraction of the Ps beam, it is necessary to understand both the fraction of induced transitions that are detected and the extent to which the transition is driven by microwave radiation. The latter was measured by varying the microwave power, as shown in Fig. 7. Here, S_B is measured with the microwave radiation on-resonance (i.e., $\nu = \nu_R$) as a function of the power (P_{input}) applied to the horn antenna. These data were fitted to a function of the form[44]

$$S_B = A\left[1 - \frac{1}{1 + bP_{input}}\right], \quad (6)$$

where A and b are fit parameters that are related to the unsaturated absorption coefficient and the saturation parameter (bP_{input}),
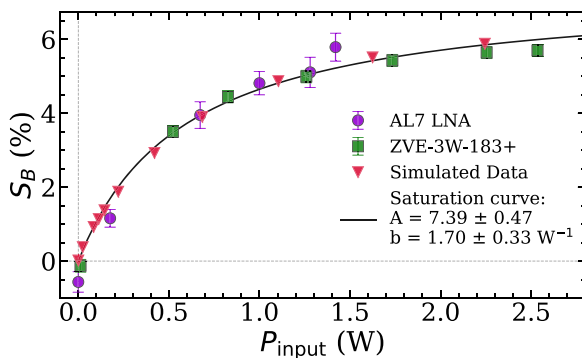

FIG. 7. S_B determined for P_{input} in the range 0–2.6 W using two amplifiers (AL7 LNA and ZVE-3W-183+) and a microwave frequency of 8.65 GHz. Also shown is a fit of Eq. (6) to both sets of experimental data in combination. The parameters extracted from the fit are listed in the legend. These data were recorded using the DLD80 detector. The simulated data were generated with QUTIP as described in Sec. III B.

respectively. These data show that saturation of the transition occurs for a horn input power of 0.59 W, with a concomitant maximum S_B value of 7.39%. This information makes it possible to determine the degree of saturation for any arbitrary horn antenna power, which in turn can be used to evaluate the fraction of the Ps beam that is in the excited state once the detected fraction has been established (see Sec. IV).

When the microwave radiation is tuned to the $2^3S_1 \rightarrow 2^3P_J$ resonance, the corresponding S_B value is proportional to the fraction of 2^3S_1 atoms in the Ps beam; this means that it can be used to measure the dependence of 2^3S_1 production on other experimental parameters.

Figure 8(a) shows the (normalized) S_B dependence on the positron beam energy. We find that 2^3S_1 production occurs over a broad range of energies, extending from a threshold value of 10 eV up to $\approx$120 eV, which defines the useful tunable range of the 2^3S_1 beam. Also shown in Fig. 8(a) is the (normalized) experimentally measured integral cross-section for Ps formation in the 2^3P_J levels $[Q_{Ps}(2P)]$ obtained by Murtagh et al.[26] The observed range of 2^3S_1 production is considerably broader than the $\approx$10 − 50 eV range of the $[Q_{Ps}(2P)]$ cross sections. We note that the calculated 2^3S_1 and 2^3P_J Ps-formation cross-sections for positron-helium
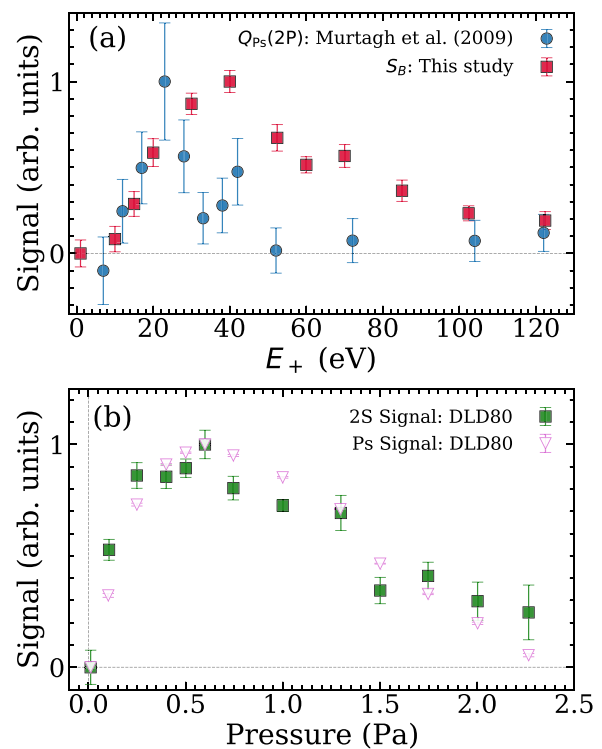

FIG. 8. (a) Dependence of the observed 2S signal on the positron beam energy (E_+), determined with a microwave radiation frequency of 8.65 GHz and an input power $P_{input} \simeq 1.4$ W. Also shown are the $Q_{Ps}(2P)$ experimental determinations of Murtagh et al.[26] Both datasets are normalized to the maximum value. (b) Pressure dependence of the 2^3S_1 signal measured using the DLD80 detector, as described in the text. In addition, the total signal from Ps formed into all states is shown.

collisions determined using the multi-center convergent close-coupling method also show a broader energy-dependence for the 2^3S_1 case.[45]

Figure 8(b) shows the (normalized) S_B dependence on the Xe gas cell pressure obtained using the DLD80 detector. Also shown are the background-subtracted total Ps beam measurements. Similar data were observed using the DLD40 detector. We find that ground state and excited state production both follow a similar pressure dependence. This is to be expected since both formation processes involve similar mechanisms, and the signal in both cases will include a trade-off between increasing Ps formation and increasing loss through scattering and breakup processes at higher gas pressures.

B. Simulations

In order to verify that the observed microwave spectroscopy data are consistent with the expected Ps properties, simulations of the excitation process were performed. Numerical calculations of the microwave fields expected in the apparatus were obtained using CST Studio.[43] This software evaluates electromagnetic fields in arbitrary configurations using the finite element method (FEM). By building a representation of the experimental chamber and microwave source, a calculation of the phase and magnitude of the electromagnetic field may be performed using a time domain solver. The results of the FEM simulation are shown in Fig. 9.

As observed in previous experiments,[42] reflections and interference effects within the vacuum chamber result in a highly

anisotropic radiation field that strongly depends on the local conditions. In the present case, the presence of the deflection plates used to stop the positron beam causes a local enhancement in the radiation intensity, as highlighted in Fig. 9(b).

Using the measured Ps velocity distributions (see Sec. II B), we generate a set of particle trajectories and extract the microwave field strength along each individual path. The trajectories were generated by sampling the (x, y) velocity distributions in Fig. 5(c) and setting the z component of the velocity according to E_{Ps} [Eq. (2)], including sampling from the positron beam energy spread (see Fig. 3). Then, following the same procedure employed in previous work,[42] we calculate the probability of a transition taking place for each atomic trajectory as a function of time. These calculations were performed by solving the Lindblad master equation[46,47] for a model four-level system using the open-source Python framework QUTIP.[48,49]

The state populations were calculated for the same frequencies and power as those used in the measurements, the latter set via a scaling factor determined from fitting the simulated saturation data to measurements, as shown in Fig. 7. From the state populations at each frequency, a simulated line shape was generated, as shown in Fig. 6, where the amplitude has been scaled to match the peak amplitude of the higher power measurement. The Stark and Zeeman shifts present in the experiment were included in the simulation by varying the relevant shifted energy levels in the different spatial regions. Since only the $\Delta M_J = 0$ transitions were included in the simulation, the shifts and associated broadening of the linewidth will be slightly underestimated,[42] but there is nevertheless good agreement between the simulated and observed linewidths. NB: If the electric field is not included in the simulation, we obtain a much narrower line shape.

As shown in Fig. 9(b), the intensity of the microwave radiation has a local maximum just after the Xe gas cell, and as a result, there is a sharp increase in the $2^3S_1 \rightarrow 2^3P_2$ transition rate in a narrow region around $z \approx 50$ mm. This is demonstrated explicitly in Fig. 10, which shows the results of a QUTIP calculation of the probability P of Ps atoms being in the initial 2^3S_1 level, averaged over all Ps atom trajectories. The calculated time evolution of the 2^3S_1 population was converted to the z dependence using the mean velocity $\langle v_z \rangle$.
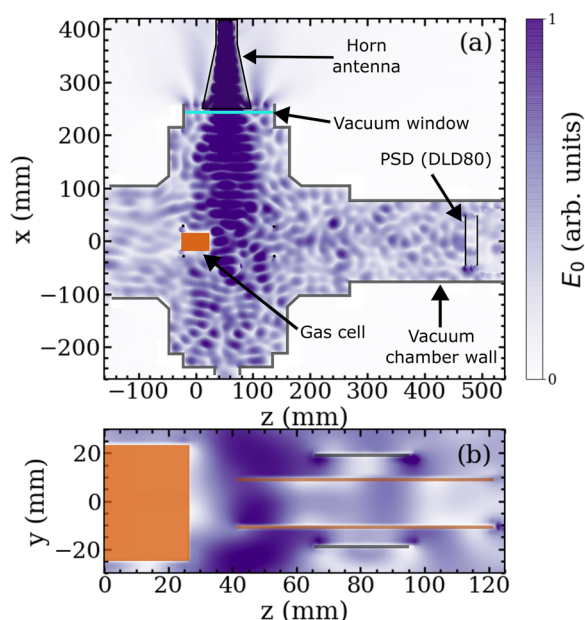

FIG. 9. (a) Top-down view of the experimental chamber and 8.65 GHz microwave radiation field in the $y = 0$ plane, simulated using numerical methods as described in the text. The position of the horn antenna, vacuum chamber walls, vacuum window, gas cell, and DLD80 detector are indicated. The deflection plates are not shown for clarity but were included in the simulation. (b) Microwave radiation field in the $x = 0$ plane at 8.65 GHz shown in the space between the deflection plates.

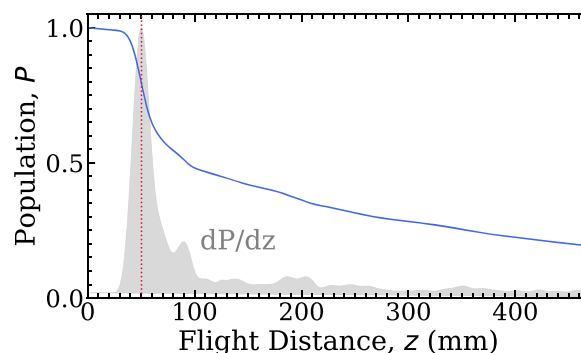**FIG. 10.** The mean 2^3S_1 state population (P) along the flight distance (z) from the center of the gas cell $(z = 0)$ to the PSD. The microwave power corresponds to $P_{input} = 1.20$ W. The shaded region indicates dP/dz for the former case, along with the position $(z = 50.4$ mm$)$ at which the $2^3S_1 \rightarrow 2^3P_2$ transition probability is highest (vertical dotted line).

These data show a rapid drop in the 2^3S_1 population near $z = 50$ mm. The z variation in this region can be seen more clearly by the shaded area in Fig. 10, which shows the rate of change of P with respect to z (i.e., dP/dz); the region where transitions are most likely to occur has a width of ≈ 20 mm and is centered on $z = 51.3$ mm.

The magnetic field in this region is ≈ 70 G, and there is a corresponding Zeeman shift of -8 MHz[33] with respect to ν_2. This region is enclosed by the deflection plates, used to prevent the positron beam from reaching the detectors, in which an electric field is present (see Sec. II A). For the 40 eV positron beam energy used in the line shape measurements, the applied electric field was 100 V/cm, which results in a Stark shift of $+46$ MHz.[31] These shifts are broadly consistent with the total measured and simulated shifts, shown in Fig. 6, that include the field variations along the entire trajectories of all atoms. We also note that anisotropic radiation fields similar to those shown in Fig. 9 are known to produce shifts in measured Ps fine structure line shapes[42] on the several MHz scale.

IV. DISCUSSION

As discussed earlier, the measured S_B values will underestimate the fraction of Ps atoms in the excited state because some atoms may still be detected, even if they are driven to the ground state by microwave radiation. If the average position for $2^3S_1 \rightarrow 2^3P_2$ transitions to occur is $z \approx 100$ mm, the mean remaining flight path to the DLD80 detector would be $z_{det} - 100 = 375$ mm. For 40 eV positrons, the corresponding Ps* flight time to the detector would then be 164 ns, and 31% of the radiation-induced ground state atoms would survive. The maximum value of S_B observed was $\approx 6\%$, and the saturation value was 7.39% (see Fig. 7). Therefore, without taking into account any possible differences in Ps and Ps* detection efficiencies, we conclude that the maximum Ps* fraction of the Ps beam is 9.68%.

The absolute Ps beam count rate observed using the present apparatus was ≈ 20 s^{-1}, giving an inferred maximum Ps* rate of ≈ 2 s^{-1}. This was obtained using a measured positron beam intensity of $\approx 50 \times 10^3$ s^{-1}, which likely corresponds to 100 000 s^{-1} when the detector efficiency is taken into account. The source strength was 400 MBq meaning that the beam intensity is on the order of 10 times lower than is possible. Therefore, with a new ^{22}Na source, a re-designed moderator assembly, and avoiding excessive collimation losses, it would be possible to generate a positron beam of $\approx 1 \times 10^7$ s^{-1}, which would correspond to Ps* rates of 400 s^{-1}. However, without employing large-scale high-intensity beam facilities (e.g., Ref. 50), this represents the maximum possible. Additional factors of two or so could be obtained by using large open area ratio MCP detectors. In previous measurements, waveguides with high transmission (90%–95%) grids were used, and a four-grid arrangement could incur a loss of $\approx 30\%$. Realistically, one could expect to obtain stable long-term Ps* rates on the order of 100 s^{-1} with straightforward improvements to the experimental apparatus.

An increase in Ps* production could be obtained by re-designing the Ps production gas cell. This was originally built to produce a narrow Ps beam for scattering measurements, with the Ps beam collimation fixed by the physical geometry of the gas cell. Relaxing the constraints of this design could allow for a higher Ps* emission fraction but at the cost of increased beam divergence, which may not be compatible with a SOF-based measurement

scheme (see Sec. V). The SOF measurements are also sensitive to the Ps* energy spread, which is mostly determined by the positron beam energy spread. The intrinsic energy width of the neon moderator ($\Delta E_+ \approx 1$ eV) is unavoidable, but positrons may also be generated from other (less efficient) moderator materials.[7] For example, positrons may be emitted from metals with negative positron affinities (e.g., single crystal Ni or W) with energy spreads $\Delta E_+ \approx 100$ meV via a work-function emission process.[51] Even colder positrons ($\Delta E_+ \approx 10$ meV) can be obtained using a cryogenic buffer gas trap.[52] Using such sources, Ps* beams with similarly narrow energy spreads could be generated, but with at least an order of magnitude reduction in intensity.

V. APPLICATION: SEPARATED OSCILLATORY FIELD MEASUREMENTS

The motivation for producing a fast Ps* beam is to make it possible to implement new measurements of the Ps fine structure (i.e., $2^3S_1 \rightarrow 2^3P_J$ transitions) using Ramsey spectroscopy.[35] Recent measurements using microwave spectroscopy[34] have revealed some systematic effects that, despite extensive modeling[53] and additional measurements,[42] have not been fully eliminated; this has limited the obtainable precision[54] to ≈ 1 MHz. One of the reasons for this is that the 50 MHz natural linewidth of the transitions requires scanning the microwave radiation frequency over a large range, for which a non-uniform system response is more likely. The Ramsey method[55] of separated oscillatory fields can partially mitigate this problem since it effectively results in a narrower line shape arising from interference effects. However, even using SOF methods, the measurements are still susceptible to variations in the frequency response of the system, albeit over a narrower range.

A recent innovation that practically eliminates this problem is the method of frequency offset separated oscillatory fields (FOSOF) developed by Vutha and Hessels.[56] This technique also uses two separated fields but introduces a small frequency offset that causes a phase shift in the Ramsey interference signal that depends linearly on the resonance frequency and the applied offset frequency. This method has two significant advantages, namely that (1) only a small frequency range around the offset has to be scanned so that the system frequency response becomes much less variable, and (2) there is a linear relationship between the phase shift and the offset frequency, making data analysis less complicated. The FOSOF method has been used to measure the hydrogen lamb shift[57] with an uncertainty of 3.2 kHz and the helium fine structure[58] (i.e., $2^3P_2 \rightarrow 2^3P_1$ transitions) with an uncertainty of 25 Hz. The FOSOF method is very well suited to Ps spectroscopy since large scanning ranges and distorted line shapes have been shown to be limiting factors in these measurements.[34]

The basis of both SOF and FOSOF measurements is that atoms (or molecules) excited to superposition states travel through a field free region before they enter a second field, tuned to drive the transitions of interest and with a well-defined phase relationship. This can be achieved using waveguides of width d separated by a distance D, where $D > d$, as indicated in Fig. 2. For monoenergetic Ps* atoms with speed v_{Ps*}, this is equivalent to atoms experiencing two pulses of duration $t = d/v_{Ps*}$ separated by time $T = D/v_{Ps}$. For Ps fine structure measurements, the resonant frequencies set the dimensions of the waveguides.[34] For convenience, we consider

here the lowest frequency transition, $v_2 = 8626.71$ MHz, in which case $d = 1.26$ cm (WR-112 waveguide). The optimal Ps* production occurs for a positron energy of $\approx$40 eV, or $v_{Ps*} = 2.3 \times 10^8$ cm/s, and the time to travel a distance $D = 5d = 6.3$ cm would be $T = 27$ ns. In the experiments we plan to conduct, the atoms initially enter the first waveguide in pure 2^3S_1 states, where they are excited to superposition states comprising both 2^3S_1 and 2^3P_2 components. Even a small admixture of 2^3P_2 character will significantly reduce the lifetime of the superposition state; in the most extreme case, the lifetime will be $\approx$3.2 ns, meaning that the 27 ns flight time would incur a 99.98% loss of signal, whereas the pure 2^3S_1 states will experience practically no loss. This immediately shows why an energetic beam is required: the Ps* produced by optical excitation in previous work[6] has energies of around 50 meV ($v_{Ps*} = 9.4 \times 10^6$ cm/s), and the equivalent flight time would be 670 ns, making the experiment impossible.

Based on the measured transverse Ps speeds (Fig. 5), we find that a WR-112 waveguide could be placed up to 20 cm away from the gas cell without Ps* beam loss. It is, therefore, possible to install a double waveguide arrangement with, for example, $5d$ separation (i.e., a total length of 8.8 cm) and still retain the full geometric acceptance for the Ps* beam, along the lines indicated in Fig. 2.

As a preliminary test, we introduced a single waveguide into the apparatus, located 46 mm from the gas cell. Lineshapes were measured using microwave radiation generated from one of two antennas placed at opposite ends of the waveguide (see Ref. 54), which makes it possible to reverse the direction of propagation of the microwave radiation and thus cancel out any Doppler shifts. The results of these measurements are shown in Fig. 11; the mean value obtained from the two waveguide measurements (for which, in contrast to the free-space measurements, there is no significant Stark shift) was $v_2 = 8627.05 \pm 2.65$ MHz, including an estimated 1 MHz systematic error related to the fields in the waveguide.[54] The magnetic field in this region was 42 G, leading to a Zeeman shift of -3.2 MHz,[33] meaning that the expected resonance frequency was 8623.51 MHz. This differs from the measurement by

3.54 MHz, which amounts to a 1.3 σ difference. This test measurement is already competitive with some of the older measurements (e.g., Ref. 59) and demonstrates that the two-waveguide Ramsey approach should be possible but that systematic effects arising from fast atoms must be carefully studied. For example, we have seen that the faster beam can exhibit relatively large Doppler shifts, so the waveguides must be carefully aligned to the beam and to each other to minimize these effects.

VI. CONCLUSIONS

A beam of 2^3S_1 Ps atoms has been formed via charge-exchange collisions between positrons in a cell filled with Xe gas. For optimized experimental parameters, we find that $\approx$10% of the Ps atoms produced in this process are at the 2^3S_1 level. The excited state component of the beam was identified using microwave radiation to drive $2^3S_1 \rightarrow 2^3P_2$ transitions. The relative positron, Ps and Ps* count rates were directly measured, taking into account in-flight decay and the position of the microwave induced transitions. The transverse velocity components of the Ps* beam were determined from the spatial distribution of the beam, observed using position sensitive detectors. The observed properties of the Ps* beam and preliminary waveguide measurements indicate that Ramsey spectroscopy will be possible using this arrangement.

AUTHOR DECLARATIONS

Conflict of Interest

The authors have no conflicts to disclose.

Author Contributions

D. M. Newson: Conceptualization (equal); Data curation (equal); Formal analysis (equal); Investigation (equal); Methodology (equal); Writing – original draft (equal); Writing – review & editing (equal). **T. J. Babij**: Conceptualization (equal); Data curation (equal); Formal analysis (equal); Investigation (equal); Methodology (equal); Writing – original draft (equal); Writing – review & editing (equal). **D. B. Cassidy**: Conceptualization (equal); Data curation (equal); Formal analysis (equal); Investigation (equal); Methodology (equal); Project administration (equal); Supervision (equal); Writing – original draft (equal); Writing – review & editing (equal).

DATA AVAILABILITY

The data that support the advances of this work are available from the corresponding author upon reasonable request.
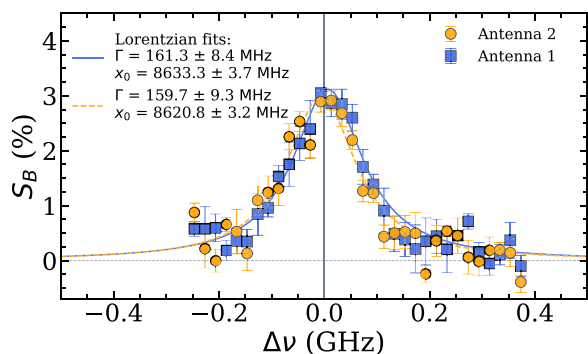

FIG. 11. S_B measured using a WR-112 rectangular waveguide with antennas located at each end. The solid and dashed curves are Lorentzian fits to the measurements performed using each antenna, as indicated in the legend. The vertical dashed line at $\Delta v = 0$ GHz corresponds to the field-free transition frequency of 8626.71 ± 0.08 MHz.

REFERENCES

[1] J. A. Wheeler, "Polyelectrons," Ann. N. Y. Acad. Sci. **48**, 219–238 (1946).

[2] S. G. Karshenboim, "Precision study of positronium: Testing bound state QED theory," Int. J. Mod. Phys. A **19**, 3879–3896 (2004).

[3] G. B. DeMaggio, W. E. Frieze, D. W. Gidley, M. Zhu, H. A. Hristov, and A. F. Yee, "Interface and surface effects on the glass transition in thin polystyrene films," Phys. Rev. Lett. **78**, 1524–1527 (1997).

[4] M. Charlton and J. W. Humberston, *Positron Physics*, 1st ed. (Cambridge University Press, Cambridge, 2001).

[5] G. Adkins, D. Cassidy, and J. Pérez-Ríos, "Precision spectroscopy of positronium: Testing bound-state QED theory and the search for physics beyond the standard model," Phys. Rep. **975**, 1–61 (2022).

[6] D. B. Cassidy, "Experimental progress in positronium laser physics," Eur. Phys. J. D **72**, 53 (2018).

[7] P. J. Schultz and K. G. Lynn, "Interaction of positron beams with surfaces, thin films, and interfaces," Rev. Mod. Phys. **60**, 701–779 (1988).

[8] A. P. Mills Jr., "Thermal activation measurement of positron binding energies at surfaces," Solid State Commun. **31**, 623–626 (1979).

[9] A. P. Mills Jr., L. Pfeiffer, and P. M. Platzman, "Positronium velocity spectroscopy of the electronic density of states at a metal surface," Phys. Rev. Lett. **51**, 1085–1088 (1983).

[10] L. Liszkay, C. Corbel, P. Perez, P. Desgardin, M. F. Barthe, T. Ohdaira, R. Suzuki, P. Crivelli, U. Gendotti, A. Rubbia, M. Etienne, and A. Walcarius, "Positronium reemission yield from mesostructured silica films," Appl. Phys. Lett. **92**, 063114 (2008).

[11] D. B. Cassidy, P. Crivelli, T. H. Hisakado, L. Liszkay, V. E. Meligne, P. Perez, H. W. K. Tom, and A. P. Mills, Jr., "Positronium cooling in porous silica measured via Doppler spectroscopy," Phys. Rev. A **81**, 012715 (2010).

[12] A. C. L. Jones, H. J. Goldman, Q. Zhai, P. Feng, H. W. K. Tom, and A. P. Mills, Jr., "Monoenergetic positronium emission from metal-organic framework crystals," Phys. Rev. Lett. **114**, 153201 (2015).

[13] T. E. Wall, A. M. Alonso, B. S. Cooper, A. Deller, S. D. Hogan, and D. B. Cassidy, "Selective production of Rydberg-Stark states of positronium," Phys. Rev. Lett. **114**, 173001 (2015).

[14] A. Deller, A. M. Alonso, B. S. Cooper, S. D. Hogan, and D. B. Cassidy, "Electrostatically guided Rydberg positronium," Phys. Rev. Lett. **117**, 073202 (2016).

[15] S. D. Hogan, "Rydberg-Stark deceleration of atoms and molecules," EPJ Tech. Instrum. **3**, 2 (2016).

[16] D. W. Gidley, R. Mayer, W. E. Frieze, and K. G. Lynn, "Glancing angle scattering and neutralization of a positron beam at metal surfaces," Phys. Rev. Lett. **58**, 595–598 (1987).

[17] G. Laricchia, S. A. Davies, M. Charlton, and T. C. Griffith, "The production of a timed tunable beam of positronium atoms," J. Phys. E: Sci. Instrum. **21**, 886 (1988).

[18] J. R. Machacek, S. J. Buckman, and J. P. Sullivan, "A pulsed positronium beam using a positron buffer gas trap," Rev. Sci. Instrum. **91**, 033311 (2020).

[19] K. Michishio, L. Chiari, F. Tanaka, N. Oshima, and Y. Nagashima, "A high-quality and energy-tunable positronium beam system employing a trap-based positron beam," Rev. Sci. Instrum. **90**, 023305 (2019).

[20] Y. Nagashima, "Experiments on positronium negative ions," Phys. Rep. **545**, 95–123 (2014).

[21] A. J. Garner, G. Laricchia, and A. Özen, "Ps beam production and scattering from gaseous targets," J. Phys. B: At., Mol. Opt. Phys. **29**, 5961 (1996).

[22] S. J. Brawley, S. E. Fayer, M. Shipman, and G. Laricchia, "Positronium production and scattering below its breakup threshold," Phys. Rev. Lett. **115**, 223201 (2015).

[23] D. M. Newson, R. Kadokura, H. Allen, S. E. Fayer, S. J. Brawley, M. Shipman, G. Laricchia, R. S. Wilde, I. I. Fabrikant, and L. Sarkadi, "Low-energy positornium scattering from O_2," Phys. Rev. A **107**, 022809 (2023).

[24] M. Shipman, S. J. Brawley, L. Sarkadi, and G. Laricchia, "Collimated positronium production from gases," Eur. Phys. J. D **68**, 75 (2014).

[25] G. Laricchia, M. Charlton, G. Clark, and T. C. Griffith, "Excited state positronium formation in low density gases," Phys. Lett. A **109**, 97–100 (1985).

[26] D. J. Murtagh, D. A. Cooke, and G. Laricchia, "Excited-state positronium formation from helium, argon, and xenon," Phys. Rev. Lett. **102**, 133202 (2009).

[27] H. A. Bethe and E. E. Salpeter, *Quantum Mechanics of One- and Two-Electron Atoms* (Springer, Berlin, 1957).

[28] A. I. Alekseev, "Two-photon annihilation of positronium in the P-state," Sov. Phys. JETP **7**, 826 (1958).

[29] A. I. Alekseev, "Three-photon annihilation of positronium in the P-state," Sov. Phys. JETP **9**, 1312 (1959).

[30] W. Demtröder, *Laser Spectroscopy*, 3rd ed. (Springer, New York, 2003).

[31] A. M. Alonso, B. S. Cooper, A. Deller, S. D. Hogan, and D. B. Cassidy, "Positronium decay from $n = 2$ states in electric and magnetic fields," Phys. Rev. A **93**, 012506 (2016).

[32] N. F. Ramsey, "Experiments with separated oscillatory fields and hydrogen masers," Rev. Mod. Phys. **62**, 541–552 (1990).

[33] L. Gurung, T. J. Babij, S. D. Hogan, and D. B. Cassidy, "Precision microwave spectroscopy of the positronium $n = 2$ fine structure," Phys. Rev. Lett. **125**, 073002 (2020).

[34] L. Gurung, T. J. Babij, J. Pérez-Ríos, S. D. Hogan, and D. B. Cassidy, "Observation of asymmetric line shapes in precision microwave spectroscopy of the positronium $2^3S_1 \rightarrow 2^JP_2$ ($J = 1, 2$) fine-structure intervals," Phys. Rev. A **103**, 042805 (2021).

[35] T. J. Babij and D. B. Cassidy, "Positronium microwave spectroscopy using Ramsey interferometry," Eur. Phys. J. D **76**, 121 (2022).

[36] A. Özen, A. J. Garner, and G. Laricchia, "Rare gas solid moderator for Ps beam at UCL," Nucl. Instrum. Methods Phys. Res., Sect. B **171**, 172–177 (2000).

[37] A. P. Mills, Jr. and E. M. Gullikson, "Solid neon moderator for producing slow positrons," Appl. Phys. Lett. **49**, 1121 (1986).

[38] P. G. Coleman, *Positron Beams and Their Applications*, 1st ed. (World Scientific Publishing, Co., Singapore, 2000).

[39] S. M. Curry, "Combined Zeeman and motional Stark effects in the first excited state of positronium," Phys. Rev. A **7**, 447 (1973).

[40] N. Zafar, G. Laricchia, M. Charlton, and T. C. Griffith, "Diagnostics of a positronium beam," J. Phys. B: At., Mol. Opt. Phys. **24**, 4661 (1991).

[41] A. Czarnecki, K. Melnikov, and A. Yelkhovsky, "Positronium S-state spectrum: Analytic results at $O(m\alpha^6)$," Phys. Rev. A **59**, 4316–4330 (1999).

[42] R. E. Sheldon, T. J. Babij, S. H. Reeder, S. D. Hogan, and D. B. Cassidy, "Microwave spectroscopy of positronium atoms in free space," Phys. Rev. A **107**, 042810 (2023).

[43] CST Studio Suite, Dassault Systèmes https://www.3ds.com/products-services/simulia/products/cst-studio-suite/.

[44] C. Foot, *Atomic Physics* (Oxford University Press, 2005).

[45] R. Utamuratov, A. S. Kadyrov, D. V. Fursa, and I. Bray, "A two-centre convergent close-coupling approach to positron–helium collisions," J. Phys. B: At., Mol. Opt. Phys. **43**, 031001 (2010).

[46] G. Lindblad, "On the generators of quantum dynamical semigroups," Commun. Math. Phys. **48**, 119–130 (1976).

[47] V. Gorini, A. Kossakowski, and E. C. G. Sudarshan, "Completely positive dynamical semigroups of N-level systems," J. Math. Phys. **17**, 821–825 (1976).

[48] J. Johansson, P. Nation, and F. Nori, "QuTiP: An open-source Python framework for the dynamics of open quantum systems," Comput. Phys. Commun. **183**, 1760–1772 (2012).

[49] J. Johansson, P. Nation, and F. Nori, "QuTiP 2: A Python framework for the dynamics of open quantum systems," Comput. Phys. Commun. **184**, 1234–1240 (2013).

[50] C. Hugenschmidt, C. Piochacz, M. Reiner, and K. Schreckenbach, "The NEPOMUC upgrade and advanced positron beam experiments," New J. Phys. **14**, 055027 (2012).

[51] D. A. Fischer, K. G. Lynn, and D. W. Gidley, "High-resolution angle-resolved positron reemission spectra from metal surfaces," Phys. Rev. B **33**, 4479–4492 (1986).

[52] M. R. Natisin, J. R. Danielson, and C. M. Surko, "A cryogenically cooled, ultra-high-energy-resolution, trap-based positron beam," Appl. Phys. Lett. **108**, 024102 (2016).

[53] L. A. Akopyan, T. J. Babij, K. Lakhmanskiy, D. B. Cassidy, and A. Matveev, "Line-shape modeling in microwave spectroscopy of the positronium $n = 2$ fine-structure intervals," Phys. Rev. A **104**, 062810 (2021).

[54] R. E. Sheldon, T. J. Babij, S. H. Reeder, S. D. Hogan, and D. B. Cassidy, "Precision microwave spectroscopy of the positronium $2^3S_1 \rightarrow 2^3P_2$ interval," Phys. Rev. Lett. **131**, 043001 (2023),

[55] N. F. Ramsey, "A new molecular beam resonance method," Phys. Rev. **76**, 996 (1949).

[56] A. C. Vutha and E. A. Hessels, "Frequency-offset separated oscillatory fields," Phys. Rev. A **92**, 052504 (2015).

[57] N. Bezginov, T. Valdez, M. Horbatsch, A. Marsman, A. C. Vutha, and E. A. Hessels, "A measurement of the atomic hydrogen Lamb shift and the proton charge radius," Science **365**, 1007–1012 (2019).

[58] K. Kato, T. D. G. Skinner, and E. A. Hessels, "Ultrahigh-precision measurement of the $n = 2$ triplet P fine structure of atomic helium using frequency-offset separated oscillatory fields," Phys. Rev. Lett. **121**, 143002 (2018).

[59] D. Hagena, R. Ley, D. Weil, G. Werth, W. Arnold, and H. Schneider, "Precise measurement of $n = 2$ positronium fine-structure intervals," Phys. Rev. Lett. **71**, 2887–2890 (1993).